

A Disturbance Margin For Quantifying Limits on Power Smoothing by Wind Turbines

Barry G. Rawn, *Member, IEEE*, Peter W. Lehn, *Senior Member, IEEE*, Manfredi Maggiore,
Member, IEEE

Abstract

Wind turbines can in principle be operated to smooth wind power fluctuations by allowing wider variations in turbine speed and generator torque to store and release energy. This ability must be constrained by turbine speed and generator torque limits. To date, work in the literature is conceptual and does not indicate what extent of smoothing is possible before component limits are reached, nor does it quantify sensitivity to variations in the input wind speed. This paper introduces a method for quantifying how much wind variation a wind turbine can absorb in variable speed mode while still being guaranteed to operate within its component limits. One can apply this method to obtain the dependence of maximum tolerable wind disturbance on the smoothing time constant, and thus make design decisions. The paper shows that the analysis of torque speed intersections, as standardly applied in electric machine theory, is of limited use for studying power smoothing. The new conclusions and design choices made available by the proposed method are illustrated with a series of computation examples. The method is shown to agree asymptotically with two limiting cases that can be calculated based on torque-intersection analysis. The method is based on new theory for computing invariance kernels for nonlinear planar systems and can be adapted to assess the robustness of other control laws.

Index Terms

Wind power generation, Nonlinear systems, Kinetic energy, State space methods, Control theory, Mathematical analysis.

B.G. Rawn is with the Department of Electrical Sustainable Energy, Delft University of Technology, Mekelweg 4, 2628 CD Delft, The Netherlands (b.g.rawn@tudelft.nl).

P.W. Lehn and M. Maggiore are with the Department of Electrical and Computer Engineering, University of Toronto, 10 King's College Road, Toronto, ON, M5S 3G4, Canada (lehn@ecf.utoronto.ca, maggiore@control.utoronto.ca).

I. INTRODUCTION

The mechanical behaviour of electric machines has traditionally been analyzed using torque-speed diagrams. Though the system dynamics are typically nonlinear, operating points are readily determined by the intersection of load torque-speed and machine torque-speed curves. Transients of such systems have commonly been viewed merely as transitions between two steady state operating points on the torque-speed plane. This simple analysis approach provides useful insights into the electro-mechanical system, but it relies on the assumption that (i) the load (or source) torque takes on a constant steady state value and (ii) electrical dynamics are much faster than the mechanical dynamics of the system.

An example of a widely-found system that violates these assumptions is the variable speed, converter-interfaced wind turbine. To achieve peak power tracking, generator torque is typically set to be an algebraic function of generator speed to establish a static curve of desired operating points in the torque-speed plane [1]. The shaft torque of the machine changes with wind speed. Thus the machine and converter are subject to a time varying torques, violating the first assumption.

With wind energy systems providing an ever growing portion of total generation, expectation of these systems to support frequency regulation in the power grid is emerging. Proposals to exploit wind turbine kinetic energy for smoothing wind power [2],[3],[4],[5], damping oscillations in power system frequency [6],[7], or counteracting momentary dips in frequency [8],[9] are the subject of growing interest in the literature. These methods all introduce electrical dynamics that, through control action, are on a time scale comparable to the mechanical dynamics. This violates the second assumption of static torque-speed analysis. In sum, static torque-speed analysis approaches are insufficient to assess this new class of system and alternative analysis techniques are required.

This paper introduces the notion of “wind disturbance margin” and provides an analysis technique to compute it. The margin in question is the largest bound on the wind input signal variation for which the turbine is guaranteed to remain within a pre-defined safe operating region. For a given mean wind speed, the margin characterizes the robustness of the energy conversion system to wind disturbances. Coupled with advanced wind speed measurement techniques [10], the margin could be used to guarantee safe operation while providing smoothing or other services that exploit turbine kinetic energy.

The computation of the margin employs a new technique that can be applied to planar nonlinear systems with a single input. The solution technique begins by first identifying the turbine’s safe operating region and mapping this region from the torque-speed plane into the state-space plane. The result is a set of safe operating points in the state plane. This set is then tested for the existence of an *invariance kernel*-

the largest set of initial conditions leading to trajectories that can never leave the set of safe operating points for a given class of wind disturbance signals. The class of wind disturbance signals is characterized only by its mean wind speed, and a bound on its range of variation. The bound is increased to find the disturbance margin, which is the largest possible bound allowed before the invariance kernel becomes empty. Instead of brute force simulation, computation of the invariance kernel employs an analytical method that calls only for the integration of a finite number of special trajectories. The paper works with the example of a wind turbine operating in variable speed mode. The turbine is subjected to wind variations that are bounded but otherwise unspecified. The generator is thus subject to a commensurate shaft torque which is also bounded but otherwise unspecified. The generator is regulated via torque control, where the torque reference is derived by low-pass filtering the generator speed. This achieves smoothing of the wind turbine output power, allowing the kinetic energy of the rotor to absorb rapid input energy changes through variation of the rotor speed. Such a system is effective in reducing the impact of wind turbine power variations on the power grid. However, too large a filtering time constant may lead to collapse [3] or overshoot of the rotor speed to the point where pitch control intervenes and causes power variations that defeat the purpose of smoothing. The simplified two-state model and the analysis presented offer a new means of assessing such power smoothing control schemes present in the literature.

The structure of the paper is as follows. In Section II the applicability of a simplified wind turbine model is discussed. Section III introduces the disturbance margin concept and associated definitions. Section IV demonstrates computation of the margin for special cases and highlights limitations of standard analysis techniques. Section V explains the planar invariance kernel analysis technique and its application to the wind turbine problem. Section VI demonstrates computation of the margin for the general case, and Sections VII provides conclusions.

II. WIND TURBINE MODELING AND CONTROL

The power conversion efficiency of a wind turbine depends on the tip-speed ratio

$$\lambda = \frac{R\omega}{v_w} \quad (1)$$

where R is the radius of the rotor disc, ω is the rotational speed of the turbine rotor, and v_w is the wind speed. There is also a dependence on the pitch angle of the blades which is not considered in this paper. The dependence of conversion efficiency on λ is shown in Fig. 1. Efficiency has a maximum at the tip-speed ratio λ_{opt} . For any larger tip speed ratio λ_{del} , conversion efficiency is lowered. A conversion

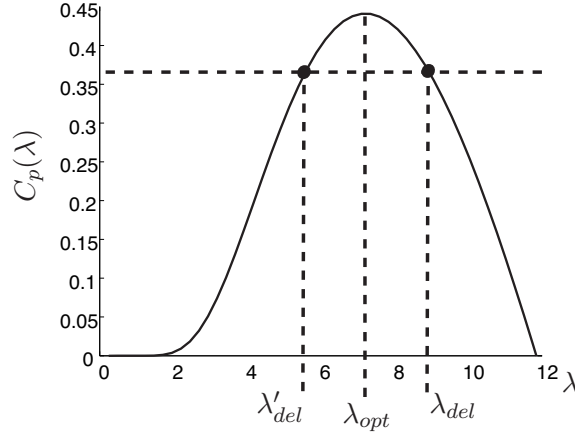


Fig. 1. Power conversion efficiency curve $C_p(\lambda)$ for optimal constant pitch angle. Optimal operation occurs at λ_{opt} , while de-loaded operation occurs for values λ'_{del} and λ_{del} .

efficiency of at least $C_p(\lambda_{del})$ is available over the range of tip-speed ratios $[\lambda'_{del}, \lambda_{del}]$. Operation at λ_{opt} is referred to as optimal, and operation away from λ_{opt} is referred to as de-loaded.

The aerodynamic torque exerted on the shaft of the wind turbine is as follows:

$$T_{aero}(\omega, v_w) = \frac{\frac{1}{2}\rho\pi R^2 C_p(\lambda) v_w^3}{\omega} \quad (2)$$

where ρ is the density of air. The dependence of the aerodynamic torque on both rotor speed and wind speed is illustrated in Fig. 2, where curves corresponding to two values of wind speed (v_w^{low} and v_w^{high}) are shown in the torque-speed plane. The values chosen are associated with variable speed operation between the rotor speeds ω^{low} and ω^{high} .

A. Control Regimes and Component Limits

There are multiple ways in which the physical limitations on wind turbine components affect wind turbine controls [1]. Wind turbines begin operating above a certain cut-in wind speed. For low wind speeds, the rotor is maintained close to its minimum speed by a steep generator torque (section (A-B) in Fig. 2). Above a rotor speed ω^{low} (greater than the minimum allowed speed by some amount [11]), variable rotor speed operation occurs (section B-C) up to a rotor speed ω^{high} (less than maximum by some amount). Above ω^{high} , both generator torque and pitch feedback controls are altered to keep rotor speed at or below the maximum value of 1.0 per-unit (C-D) [12]. The maximum torque and rotor speed (D) are reached at the rated wind speed. For wind speeds above rated, electric power is limited to the

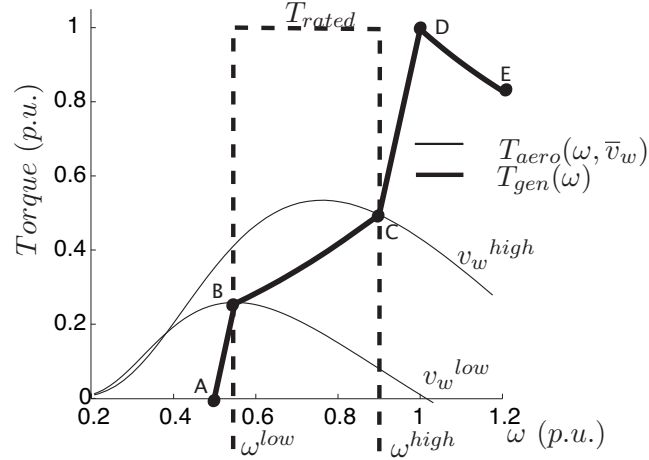


Fig. 2. Aerodynamic (solid) and generator torque-speed curves (thick) for variable speed wind turbine. Letters label operating points where various control schemes become active. Safe region for variable speed operation is enclosed by a dashed box.

rated value for the wind turbine using a constant power generator torque curve (D-E) and the adjustment of pitch to reduce aerodynamic torque.

In variable rotor speed operation (B-C), pitch is set to the optimal value and pitch control is not active [13]. Rotor speed is free to vary between speeds ω^{low} and ω^{high} , provided the maximum torque limit T_{rated} is never exceeded. The generator torque T_{gen} in modern variable speed wind turbines is established through control of power electronics [14]. Between the points B and C T_{gen} is set to:

$$T_{gen}(\omega) = k_{load}(\lambda_*)\omega^2 \quad (3)$$

$$k_{load}(\lambda_*) = \frac{1}{2}\rho\pi C_p(\lambda_*) \frac{R^5}{\lambda_*^3} \quad (4)$$

where λ_* is a desired tip-speed ratio. The generator torque curve in the torque speed plane is often referred to as the *load curve*. The load curve is intended to allow the rotor speed to continually adjust to new setpoints as the wind speed changes. The choice of (3)-(4) has the effect that for a constant wind speed the efficiency $C_p(\lambda_*)$ is reached in the steady state.

B. Simplified Dynamic Model for Power Smoothing

For control design related to power smoothing, a model of wind turbine dynamics in the variable speed range (B-C) can neglect the pitch control, which is inactive, and can be very simple [15],[13], consisting only of the single nonlinear differential equation for rotor speed dynamics:

$$J \frac{d\omega}{dt} = T_{aero}(\omega, v_w) - T_{gen} \quad (5)$$

where J is the rotational inertia of the turbine hub and generator. For operation at and above rated wind speed (D-E), structural vibrational modes such as the tower deflection are usually also modelled because of their interaction with pitch control [13] and relatively large excitation at high wind speeds [16]. However, in variable speed operation (B-C) the excitation is much smaller and not enough to warrant extra pitch actuator wear [16]. Tower deflections also have little discernable effect on rotor speed [17]. For these reasons tower and other structural modes can be safely excluded from this model, as is widely done for control design purposes [18].

The objective of power smoothing is to exploit variable speed operation to absorb wind power fluctuations using the rotational kinetic energy of the turbine. The concept has been explored with control schemes that set constant power or torque [4],[5] or that introduce a low-pass filter into the signal path used to generate these control references [2],[3],[19]. Most of these works acknowledge that depending on the chosen time constant of smoothing and amount of de-loading, instability may result from power smoothing. None of these works quantify how much smoothing is practically viable.

To study how power smoothing controls should safely be designed, this paper examines the controller introduced in [2]. A low-pass filter is applied to a measurement of rotor speed, and a new variable ω_{filt} is used to generate a power reference. The power reference is extracted regardless of rotor speed by setting the torque command depicted in Fig. 3, which equals the desired level of power divided by the unfiltered rotor speed ω :

$$T_{gen}(\omega, \omega_{filt}) = \frac{k_{load}(\lambda_*) \omega_{filt}^3}{\omega}. \quad (6)$$

Dynamics are now described by two differential equations:

$$\begin{aligned} J \frac{d\omega}{dt} &= T_{aero}(\omega, v_w) - \frac{k_{load}(\lambda_*) \omega_{filt}^3}{\omega} \\ \tau \frac{d\omega_{filt}}{dt} &= \omega - \omega_{filt}. \end{aligned} \quad (7)$$

where τ is the time constant of rotor speed filtering. The choice of a power reference with a low-pass filter in the signal path has two advantages. First, such control structures are already in place (with small time constants) in some industry implementations [7],[20]. Second, in the limit for large τ the model (7) corresponds with constant power smoothing schemes studied in literature [4],[5].

C. Limiting Cases

Two limiting cases of speed filtering can be considered to provide insight into system operation. For $\tau = 0$, $\omega_{filt} = \omega$ and the generator torque (6) simplifies to the standard maximum power tracking law

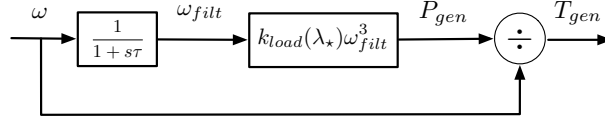


Fig. 3. Block diagram of power smoothing generator torque $T_{gen}(\omega, \omega_{filt})$ based on filtered rotor speed [2].

(3), in which case the rotor speed variations are dictated by:

$$J \frac{d\omega}{dt} = T_{aero}(\omega, v_w) - k_{load}(\lambda_*) \omega^2. \quad (8)$$

For $\tau = \infty$, ω_{filt} is a constant ω_{filt}^0 , and rotor speed variations are instead dictated by

$$J \frac{d\omega}{dt} = T_{aero}(\omega, v_w) - \frac{k_{load}(\lambda_*) (\omega_{filt}^0)^3}{\omega}. \quad (9)$$

Setting ω_{filt}^0 to the steady state rotor speed associated with a wind speed \hat{v}_w

$$\omega_{filt}^0 = \frac{\lambda_*}{R} \hat{v}_w. \quad (10)$$

simplifies (9) to

$$J \frac{d\omega}{dt} = \frac{\frac{1}{2} \rho \pi R^2}{\omega} (C_p(\lambda) v_w^3 - C_p(\lambda_*) \hat{v}_w^3) \quad (11)$$

where \hat{v}_w sets the constant power level demanded and could be, for example, set to the mean or minimum value of wind speed expected in a certain period, as is suggested in other work [4],[5].

When the generator torque control law has no dynamics of its own as in (8) or (11), movement in the torque speed-plane is confined to the load curve. When instead the control input (6) is employed, movement in the torque-speed plane depends on dynamics of both ω and ω_{filt} and can leave the load curve.

III. WIND DISTURBANCE MARGIN DEFINITION

In this work, we consider a wind speed input

$$v_w(t) = \bar{v}_w + \delta v_w(t) \quad (12)$$

where \bar{v}_w is a mean speed, and $\delta v_w(t)$ is a deviation.

To define the wind disturbance margin, we use a number of sets [21]. We begin by defining the collection of all wind deviations bounded from above by a constant Δ .

Definition 1: Class $\mathcal{N}(\Delta)$ of Wind Deviation Signals

Denote by $\mathcal{N}(\Delta)$ the class of all wind deviations bounded by Δ :

$$\mathcal{N}(\Delta) \triangleq \{\delta v_w(t) : |\delta v_w(t)| \leq \Delta \text{ for all } t \in \mathbb{R}\}, \quad (13)$$

so that

$$v_w(t) \in [\bar{v}_w - \Delta, \bar{v}_w + \Delta]. \quad (14)$$

Next, we define the set of all feasible states of the wind turbine model (7) corresponding to arbitrary *constant* wind speeds in the interval $[\bar{v}_w - \Delta, \bar{v}_w + \Delta]$.

Definition 2: Equilibrium Set \mathcal{E}

The *equilibrium set* $\mathcal{E}(\Delta, \bar{v}_w, \lambda_*)$ of (7) is the collection of all equilibria of (7) assuming that the wind is constant, and that its value ranges over the interval $[\bar{v}_w - \Delta, \bar{v}_w + \Delta]$. In other words,

$$\mathcal{E}(\Delta, \bar{v}_w, \lambda_*) \triangleq \left\{ (\omega, \omega_{filt}) : \omega = \frac{\lambda_*}{R} v_w^0, \omega_{filt} = \omega, v_w^0 \in [\bar{v}_w - \Delta, \bar{v}_w + \Delta] \right\}. \quad (15)$$

The equilibrium set $\mathcal{E}(\Delta, \bar{v}_w, \lambda_*)$ is depicted on the ω - ω_{filt} state plane in Fig. 4 for a specific choice of Δ , \bar{v}_w , and λ_* . Also shown in Fig. 4 is a dashed line corresponding to the rotor speed limits and torque limits of the machine. The rotor speed limits are the same as those defined in Fig. 2. Imposing a limit on the absolute value of generator torque T_{gen} to be less or equal than the rated torque T_{rated} requires in turn a limit on the filter state ω_{filt} , through the relation (6). The necessary limits on ω_{filt} can be obtained by setting $T_{gen} = \pm T_{rated}$ and solving for ω_{filt} . Outside of these limits, safety controls will intervene to maintain rotor speed through pitch action or to limit converter currents. Intervention by safety controls will disrupt the behaviour intended by the control law (6). The rotor speed limits, combined with the machine torque limits, form bounds on a region in the ω - ω_{filt} state plane. The region of free operation whose borders are enforced by safety controls will be called the **safety set**.

Definition 3: Safety Set \mathcal{S}

$$\mathcal{S} \triangleq \left\{ (\omega, \omega_{filt}) : \omega^{low} \leq \omega \leq \omega^{high}, -\sqrt[3]{\frac{T_{rated}\omega}{k_{load}(\lambda_*)}} \leq \omega_{filt} \leq \sqrt[3]{\frac{T_{rated}\omega}{k_{load}(\lambda_*)}} \right\}. \quad (16)$$

In this paper, we will also refer to this set's boundary using the notation $\partial\mathcal{S}$.

For a chosen control law, the wind turbine's state over time will be determined by the dynamical equations and the wind signal input, which we have restricted for this work to signals of the class

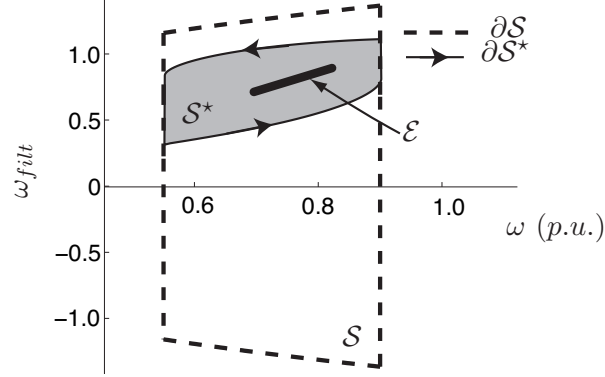


Fig. 4. Safety set \mathcal{S} , equilibrium set \mathcal{E} and the invariance kernel \mathcal{S}^* that define disturbance margin \mathcal{M} for the system (7).

defined in Definition 1. We will associate the desired behaviour of the wind turbine over time with the existence of a **positively invariant set**. To this end, let $x(t, x_0)$ denote the solution of (7) with initial condition x_0 . Fix \bar{v}_w and Δ and consider system (7) with a wind signal $v_w(t) = \bar{v}_w + \delta v_w(t)$.

Definition 4: Positively Invariant Set \mathcal{I}

A set $\mathcal{I} \in \mathbb{R}^2$ is said to be *positively invariant* for (7) if $\forall x_0 \in \mathcal{I}$, and $\forall \delta v_w(t) \in \mathcal{N}(\Delta)$, $x(t, x_0) \in \mathcal{I}$, $\forall t \geq 0$.

Initial conditions belonging to a positively invariant set produce trajectories that can never leave that set, no matter what wind signal in the class $v_w(t) = \bar{v}_w + \delta v_w(t) \in \mathcal{N}(\Delta)$ affects the wind turbine. The definition of a positively invariant set can analogously be made for the control law (3) and dynamics (8), or other control laws.

Of particular interest are positively invariant sets contained in the safety set. Indeed, if \mathcal{I} is such a positively invariant set, initial conditions in \mathcal{I} lead to solutions of (7) that satisfy the safety limits of the turbine for any wind signal in the class $v_w(t) = \bar{v}_w + \delta v_w(t)$, with $\delta v_w(t) \in \mathcal{N}(\Delta)$. In this context, it is natural to look for the *largest* positively invariant set contained in the safe set.

Definition 5: Safety Set Invariance Kernel \mathcal{S}^ :*

Given the safety set \mathcal{S} in Definition 3, a chosen bound Δ , a mean wind speed \bar{v}_w , a desired tip-speed ratio λ_* , and a filter time constant τ , the set $\mathcal{S}^*(\Delta, \bar{v}_w, \lambda_*, \tau)$ is the maximal set contained in the wind turbine safety set \mathcal{S} that is positively invariant for (7).

Given a class of wind signals and values of λ_* and τ , if it happens that the invariance kernel \mathcal{S}^* is empty, then for all initial conditions in \mathcal{S} , there exists a wind signal making the solution $x(t)$ exit the safety

set. In such a situation we would conclude that the wind turbine cannot tolerate arbitrary wind signals in the stated class. A class of wind signals is therefore feasible for the wind turbine if the associated invariance kernel is not empty. More precisely, given values of $\Delta, \bar{v}_w, \lambda_*$, and τ , the least one must require in order to conclude that the turbine can tolerate arbitrary wind signals $v_w(t) = \bar{v}_w + \delta v_w(t)$ with $\delta v_w(t) \in \mathcal{N}(\Delta)$, is that \mathcal{S}^* contains the equilibrium set \mathcal{E} associated with all constant winds in the interval $[\bar{v}_w - \Delta, \bar{v}_w + \Delta]$. This observation inspires our definition of wind disturbance margin.

Definition 6: Wind Disturbance Margin \mathcal{M} :

Given the safety set \mathcal{S} , a mean wind speed \bar{v}_w , a desired tip-speed ratio λ_* , and a filter time constant τ , the wind disturbance margin $\mathcal{M}(\bar{v}_w, \lambda_*, \tau)$ is the largest value of Δ for which the invariance kernel $\mathcal{S}^*(\Delta, \bar{v}_w, \lambda_*, \tau)$ is non-empty and contains the equilibrium set $\mathcal{E}(\Delta, \bar{v}_w, \lambda_*)$.

IV. WIND DISTURBANCE MARGIN COMPUTATION: SPECIAL CASES

The boundary cases of power smoothing with $\tau = 0$ or $\tau = \infty$ are degenerate cases where the variable ω_{filt} is either equal ω , or is constant, with no dynamics. Analysis of these cases can be conducted in the torque speed plane by studying the single differential equation (8) or (11). Because there is only one state, the sets \mathcal{S}, \mathcal{E} , and \mathcal{S}^* are all intervals of the real line. A simplification of the safety set results because the generator torque depends only on ω , and the torque limit T_{rated} is not reached for any rotor speed in $[\omega^{low}, \omega^{high}]$. Therefore ensuring that rotor speed is contained in $[\omega^{low}, \omega^{high}]$ will also guarantee torque limits are not exceeded. The safety set \mathcal{S} reduces to:

$$\mathcal{S} \triangleq \left\{ \omega : \omega^{low} \leq \omega \leq \omega^{high} \right\}. \quad (17)$$

The cases $\tau = 0$ and $\tau = \infty$ will be used to introduce the concept of the disturbance margin and show the limitations of torque-speed analysis.

A. Degenerate cases $\tau = 0$ and $\tau = \infty$

For the degenerate case $\tau = 0$, the effect of all wind deviations in $\mathcal{N}(\Delta)$ can be examined using the pair of extreme aerodynamic torque curves shown in Fig. 5 (light solid), along with the generator torque given by (3) and also shown (heavy solid). For the practical range of tip-speed ratios encountered, $T_{aero}(\omega, v_w)$ depends monotonically on v_w . Consequently the extreme values of $T_{aero}(\omega, v_w)$ occur at the wind speeds $\bar{v}_w - \Delta$ and $\bar{v}_w + \Delta$. The equilibrium set \mathcal{E} is defined for the steady states of (8) instead of the steady states of (7) and coincides with the interval $[\omega_-, \omega_+]$.

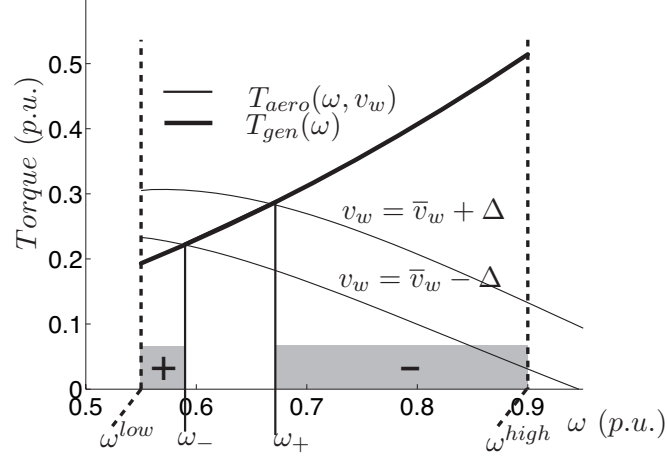


Fig. 5. Determination of \mathcal{S}^* for $\tau = 0$ based on intervals of guaranteed acceleration and deceleration (shaded). $\mathcal{S} = [\omega^{low}, \omega^{high}]$, $\mathcal{E} = [\omega_-, \omega_+]$, $\mathcal{S}^* = \mathcal{S}$.

The invariance kernel \mathcal{S}^* is an interval whose torque-speed points are associated with torque-speed intersections. As depicted in Fig. 5, for all time and for any deviation in $\mathcal{N}(\Delta)$, there are some rotor speeds that experience a consistent acceleration (shaded +) or deceleration (shaded -). These shaded intervals are bounded at one end by one of the limiting speeds ω^{low} or ω^{high} , and at the other end by a rotor speed corresponding to torque-speed intersections of the extreme aerodynamic torque curves. For the single pair of intersections occurring for the case $\tau = 0$, the intersection associated with the lowest wind speed $\bar{v}_w - \Delta$ is ω_- and with the highest wind speed $\bar{v}_w + \Delta$ is ω_+ . At the lower speed ω^{low} , acceleration is consistently experienced, and at the upper speed ω^{high} , deceleration is consistently experienced. For the value of Δ chosen in Fig. 5, the rotor speed can not be driven out of the entire safe interval $[\omega^{low}, \omega^{high}]$. Therefore \mathcal{S}^* is $[\omega^{low}, \omega^{high}]$.

The wind disturbance margin \mathcal{M} for the case $\tau = 0$ is the largest bound Δ that still ensures $[\omega^-, \omega^+]$ is contained within the safety set $[\omega^{low}, \omega^{high}]$.

$$\mathcal{M}(\bar{v}_w, \lambda_*, 0) = \begin{cases} v_w^{high} - \bar{v}_w, & \bar{v}_w > \frac{R}{\lambda_*} \frac{(\omega^{high} - \omega^{low})}{2} \\ \bar{v}_w - v_w^{low}, & \bar{v}_w \leq \frac{R}{\lambda_*} \frac{(\omega^{high} - \omega^{low})}{2} \end{cases} \quad (18)$$

where v_w^{low} and v_w^{high} are defined as follows:

$$v_w^{low} = \frac{R\omega^{low}}{\lambda_*}, \quad (19)$$

$$v_w^{high} = \frac{R\omega^{high}}{\lambda_*}. \quad (20)$$

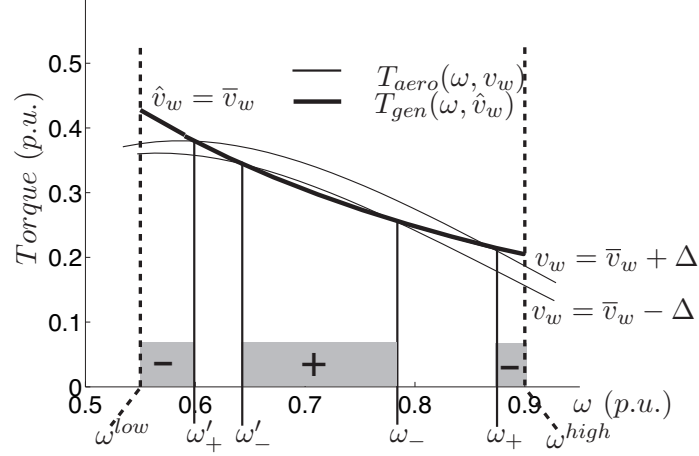


Fig. 6. Determination of \mathcal{S}^* for $\tau = \infty$ based on intervals of guaranteed acceleration and deceleration (shaded). $\mathcal{S} = [\omega^{low}, \omega^{high}]$, $\mathcal{E} = [\omega_-, \omega_+]$, $\mathcal{S}^* = [\omega'_-, \omega^{high}]$

For the degenerate case $\tau = \infty$, analogous arguments apply using the aerodynamic torque curve and generator torque indicated in (11). The equilibrium set \mathcal{E} is again $[\omega_-, \omega_+]$, but there are two complications. Fig. 6 shows an example where de-loading has set conversion efficiency to 10% lower than optimal. The first complication is that two torque speed intersections exist for each wind speed. Thus the two extreme aerodynamic torque curves produce two pairs of intersections ω_+, ω'_+ and ω_-, ω'_- . The second complication is that for each $\hat{v}_w \in [\bar{v}_w - \Delta, \bar{v}_w + \Delta]$ there is a corresponding generator curve. Fig. 6 depicts the case $\hat{v}_w = \bar{v}_w$.

When operating with de-loading, the constant power extracted is less than or equal to the maximum available for a range of speeds below \hat{v}_w . For all possible wind deviations in $\mathcal{N}(\Delta)$ and the choice of \hat{v}_w depicted in Fig. 6, although the wind deviations cause deceleration at ω^{low} , acceleration is experienced at ω'_- , and deceleration at ω^{high} . Thus, \mathcal{S}^* is not empty for the case shown- it is equal $[\omega'_-, \omega^{high}]$.

However, for a sufficiently large drop in wind speed, an intersection does not exist between $T_{gen}(\omega, \hat{v}_w)$ and $T_{aero}(\omega, \bar{v}_w - \Delta)$. When $\hat{v}_w = \bar{v}_w + \Delta$, the drop required is the smallest. In this case, the intersections at ω_- and ω'_- exist only deviations smaller than

$$\bar{\Delta}(\bar{v}_w) \triangleq \bar{v}_w \frac{\left(1 - \sqrt[3]{\frac{C_p(\lambda_*)}{C_p(\lambda_{opt})}}\right)}{\left(1 + \sqrt[3]{\frac{C_p(\lambda_*)}{C_p(\lambda_{opt})}}\right)}, \quad (21)$$

which is the deviation for which $\omega'_- = \omega_-$.

It is also necessary to analyze the deviations in wind speed for which $\omega_- = \omega^{low}$ or for which $\omega_+ = \omega^{high}$. Referring to Fig. 6, the rotor speed ω_+ is the intersection point between the aerodynamic

torque curve for $v_w = \bar{v}_w + \Delta$ and the generator torque curve. The largest value of ω_+ is obtained when $\hat{v}_w = \bar{v}_w - \Delta$. An implicit definition for $\Delta^{high}(\bar{v}_w)$, the deviation for which $\omega_+ = \omega^{high}$ in the steady state, can be identified. Substituting into (11) as follows: (1) for λ , $\omega = \omega^{high}$, v_w and \hat{v}_w as just mentioned, and $\Delta = \Delta^{high}(\bar{v}_w)$, yields

$$C_p \left(\frac{R\omega^{high}}{\bar{v}_w + \Delta^{high}(\bar{v}_w)} \right) \frac{1}{\left(\frac{\bar{v}_w - \Delta^{high}(\bar{v}_w)}{\bar{v}_w + \Delta^{high}(\bar{v}_w)} \right)^3} = C_p(\lambda_\star). \quad (22)$$

Similarly, a deviation $\Delta^{low}(\bar{v}_w)$ is associated with the rotor speed ω_- , which is the intersection point between the aerodynamic torque curve for $v_w = \bar{v}_w - \Delta$ and the generator torque curve. The smallest value of ω_- is obtained when $\hat{v}_w = \bar{v}_w + \Delta$, leading to a second implicit definition:

$$C_p \left(\frac{R\omega^{low}}{\bar{v}_w - \Delta^{low}(\bar{v}_w)} \right) \frac{1}{\left(\frac{\bar{v}_w + \Delta^{low}(\bar{v}_w)}{\bar{v}_w - \Delta^{low}(\bar{v}_w)} \right)^3} = C_p(\lambda_\star). \quad (23)$$

For a given mean wind speed, it is the smallest of the three deviations $\Delta^{low}(\bar{v}_w)$, $\bar{\Delta}(\bar{v}_w)$, and $\Delta^{high}(\bar{v}_w)$ that determines the wind disturbance margin. The wind disturbance margin \mathcal{M} for the case $\tau = \infty$ is:

$$\mathcal{M}(\bar{v}_w, \lambda_\star, \infty) = \begin{cases} \Delta^{low}(\bar{v}_w) & \bar{v}_w < \bar{v}_w^{low} \\ \bar{\Delta}(\bar{v}_w), & \bar{v}_w^{low} < \bar{v}_w < \bar{v}_w^{high} \\ \Delta^{high}(\bar{v}_w), & \bar{v}_w^{high} \leq \bar{v}_w \end{cases} \quad (24)$$

The threshold value \bar{v}_w^{low} of mean wind speed where $\Delta^{low}(\bar{v}_w)$ gives over to $\bar{\Delta}(\bar{v}_w)$ is where the deviations become equal. This threshold speed can be defined implicitly by setting $\Delta^{low}(\bar{v}_w) = \bar{\Delta}(\bar{v}_w)$ in (23) and substituting \bar{v}_w^{low} for \bar{v}_w :

$$C_p \left(\frac{R\omega^{low}}{2\bar{v}_w^{low}} \left(1 + \sqrt[3]{\frac{C_p(\lambda_{opt})}{C_p(\lambda_\star)}} \right) \right) \frac{1}{\left(\frac{1 + \sqrt[3]{\frac{C_p(\lambda_{opt})}{C_p(\lambda_\star)}}}{1 + \sqrt[3]{\frac{C_p(\lambda_\star)}{C_p(\lambda_{opt})}}} \right)^3} = C_p(\lambda_\star). \quad (25)$$

Similarly the threshold value \bar{v}_w^{high} where $\Delta^{high}(\bar{v}_w)$ takes over from $\bar{\Delta}(\bar{v}_w)$ is also defined implicitly:

$$C_p \left(\frac{R\omega^{high}}{2\bar{v}_w^{high}} \left(1 + \sqrt[3]{\frac{C_p(\lambda_\star)}{C_p(\lambda_{opt})}} \right) \right) \frac{1}{\left(\frac{1 + \sqrt[3]{\frac{C_p(\lambda_\star)}{C_p(\lambda_{opt})}}}{1 + \sqrt[3]{\frac{C_p(\lambda_{opt})}{C_p(\lambda_\star)}}} \right)^3} = C_p(\lambda_\star). \quad (26)$$

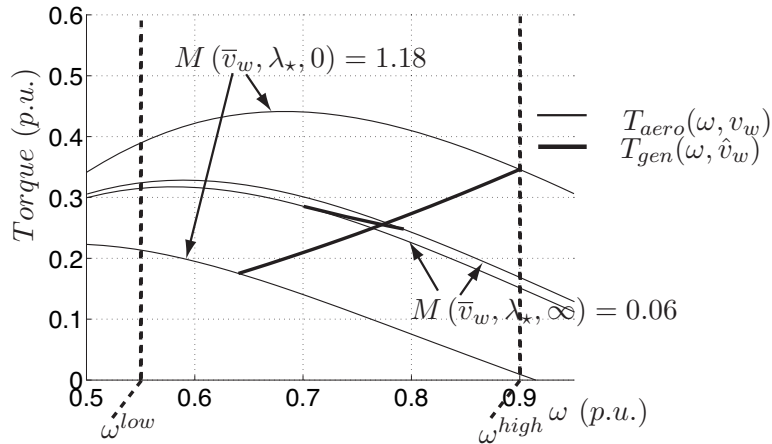


Fig. 7. Torque-speed curves used to compute disturbance margin $\mathcal{M}(\bar{v}_w, \lambda_*, \tau)$ for systems (8) ($\tau = 0$) and (11) ($\tau = \infty$) at $\bar{v}_w = 7$ and a de-loading of 5%, $\lambda_* = 7.74$.

B. Limitations of Torque Speed Intersection Analysis

The computations of \mathcal{M} available from analysis of the limiting cases of τ are illustrated for an example in Fig. 7. At the chosen mean wind speed and de-loading, analysis of the case $\tau = 0$ suggests that wind deviations in $\mathcal{N}(\Delta)$ for $\Delta \leq 1.18$ are acceptable ($\mathcal{M} = 1.18$). Larger disturbances cause the rotor speed to exceed ω^{high} . Analysis of the case $\tau = \infty$ suggests that only values of $\Delta \leq 0.06$ are acceptable ($\mathcal{M} = 0.06$). Larger disturbances allow collapse of the rotor speed to occur, because the torque-speed intersection no longer exists for some wind speeds in the range $[\bar{v}_w - \Delta, \bar{v}_w + \Delta]$. The disturbance margin \mathcal{M} quantifies robustness of a control algorithm to wind disturbances. For the degenerate cases of $\tau = 0$ or $\tau = \infty$ shown in Fig. 7, torque-speed analysis is sufficient to exactly compute the disturbance margin.

The cases shown in Fig. (7) are of limited help in assessing the case of $0 < \tau < \infty$. Fig. 8 shows that the steady state response of the system (7) with the same \bar{v}_w and λ_* but with $\tau = 8s$ (dashed) is stable for a periodic disturbance with amplitudes up to 0.6. Since the torque-speed variation reaches the upper rotor speed limit ω^{high} , $\mathcal{M}(\bar{v}_w, \lambda_*, 8)$ is surely no greater than 0.6, well below $\mathcal{M}(\bar{v}_w, \lambda_*, 0)$. However the margin most likely far exceeds an amplitude of 0.06 as determined from $\mathcal{M}(\bar{v}_w, \lambda_*, \infty)$. A computation of \mathcal{M} 's dependence on τ requires the analysis technique presented in the next section.

V. PLANAR INVARIANCE KERNEL ANALYSIS

A wind turbine subjected to a generator torque based on a filtered rotor speed has dynamics described by two state variables, as introduced in (7). This case involves a two dimensional vector field in the

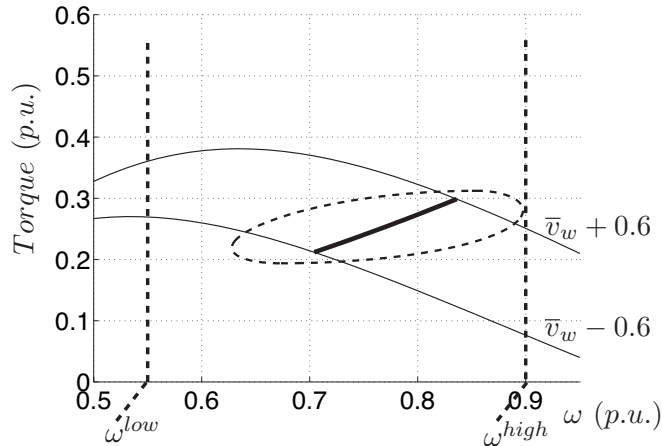


Fig. 8. Response of system (7) with $\tau = 8s$ (dashed) compared with response of (8) (thick solid) to periodic wind deviation around a mean wind speed $\bar{v}_w = 7m/s$ with an amplitude of $0.6m/s$ and a period of $40s$, and the same mean wind speed and de-loading as in Fig. 7. Thin solid lines show aerodynamic torque speed curves for $\bar{v}_w \pm 0.6$.

(ω, ω_{filt}) state plane. It will be helpful to discuss this vector field in abstract form:

$$\dot{x} = f(x) + g(x) h(x, u) \quad (27)$$

where $x = [x_1, x_2]$ with $x_1 = \omega$, $x_2 = \omega_{filt}$, $u = v_w$, and

$$f(x) = \begin{bmatrix} -\frac{k_1 x_2^3}{x_1} \\ \frac{x_1 - x_2}{k_2} \end{bmatrix} \quad (28)$$

$$g(x) = \begin{bmatrix} \frac{k_3}{x_1} \\ 0 \end{bmatrix} \quad (29)$$

$$h(x, u) = C_p \left(\frac{k_4 x_1}{u} \right) u^3 \quad (30)$$

with constants $k_1 = k_{load}(\lambda_*)/J$, $k_2 = \tau$, $k_3 = \frac{1}{2}\rho\pi R^2/J$, $k_4 = R$, and function $C_p(\lambda)$ as shown in Fig. 3. This choice of $g(x)$ and $h(x, u)$ highlights the slight difference between (27) and a system affine in the control u .

A. Concepts and Definitions

If the input u is bounded (as per (14)) then at each point in the state plane there is a cone of possible directions for the vector field (27). This is depicted in Fig. 9. Since $f(x)$ and $g(x)$ are fixed for a given x , the spread of the cone depends on the known vector $g(x)$ scaled by $h(x, u)$, which varies between

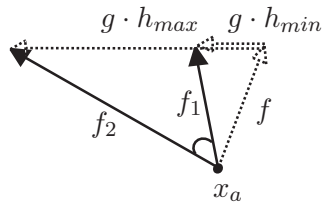


Fig. 9. Cone of possible variations due to bounded wind variation at a point x_a . Representation using original vectors f and g (dashed) is equivalent to convex combination of vectors f_1 and f_2 (solid).

h_{min} and h_{max} . For the wind turbine system, u corresponds to the wind speed. For the C_p curve and domain of wind and rotor speeds studied in this paper, $h(x, u)$ has a monotonic dependence on u . This fact is established in the Appendix, where a condition to check monotonicity for a wind turbine model is derived from the function $h(x, u)$ and numerically checked. Thus extreme values h_{min} and h_{max} and therefore also the edges of the cone are obtained for the extreme values of the input u .

Instead of working with the functions $f(x)$ and $g(x)$, it is more convenient to work with the vectors that are the edges of the cone in Fig. 9. These edge vectors are given by:

$$f_1(x) = f(x) + g(x) h_{min}(x) \quad (31)$$

$$f_2(x) = f(x) + g(x) h_{max}(x). \quad (32)$$

The right-hand side of (27) can be written as a convex combination of $f_1(x)$ and $f_2(x)$

$$\dot{x} = \alpha f_1(x) + (1 - \alpha) f_2(x). \quad (33)$$

with $\alpha \in [0, 1]$. Varying $\alpha \in [0, 1]$ in (33) corresponds to varying $u \in [\bar{v}_w - \Delta, \bar{v}_w + \Delta]$ in (27).

We are in search of the invariance kernel, \mathcal{S}^* , shown in Fig. 4. It has been shown [22] that the invariance kernel is a closed set with a boundary $\partial\mathcal{S}^*$ that is the union of parts of the boundary $\partial\mathcal{S}$ of the safety set \mathcal{S} , and of trajectories of the fields f_1 and f_2 . On $\partial\mathcal{S}^*$, we require both edges of the cone to either point to the interior of \mathcal{S}^* or to be tangent to $\partial\mathcal{S}^*$. Since \mathcal{S}^* is the largest possible positively invariant subset of \mathcal{S} at least one of the edge fields will be tangent to the boundary $\partial\mathcal{S}^*$ for those pieces not coinciding with $\partial\mathcal{S}$ [22].

We proceed with identification of \mathcal{S}^* by first discerning between the left and the right edges of the cone. Fig. 10 illustrates the need for further definition. At one point x_a , the cone is found to the left of the field $f_1(x)$. But for a nearby point x_b , the two fields could be parallel, and at another point x_c , the cone might now be found to the right of $f_1(x)$. The plane can be partitioned into three sets based on the

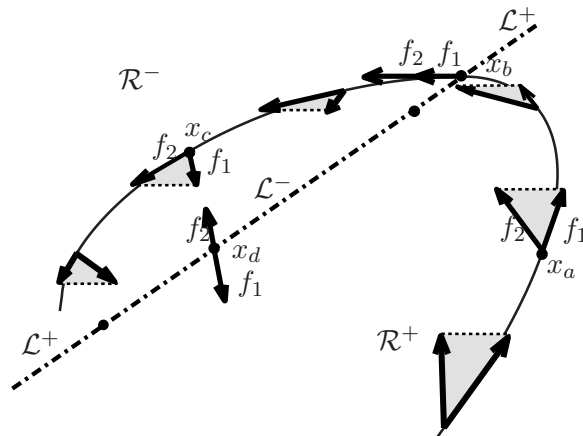


Fig. 10. Example of extremal trajectory of $f_L(x)$ (thin solid) and relation between f_1 and f_2 on the sets \mathcal{R}^+ , \mathcal{R}^- , and \mathcal{L} (dash-dot line).

possible angle relation between $f_1(x)$ and $f_2(x)$. Points such as x_a where $f_2(x)$ points to the left-hand side of $f_1(x)$ ($\det[f_1, f_2] > 0$) comprise a set \mathcal{R}^+ . Points such as x_c where $f_2(x)$ points instead to the right-hand side of f_1 ($\det[f_1, f_2] < 0$) comprise a set \mathcal{R}^- . Points where the vectors $f_1(x)$ and $f_2(x)$ are parallel (x_b) or anti-parallel (x_d) comprise the *collinearity set*.

Definition 7: We define the **collinearity set** \mathcal{L} and its subsets using the determinant and dot product as follows:

$$\mathcal{L} = \{x \in \mathbb{R}^2 : \det[f_1(x) \ f_2(x)] = 0\}.$$

with subsets $\mathcal{L}^+ = \{x \in \mathcal{L} : \langle f_1(x), f_2(x) \rangle > 0\}$, $\mathcal{L}^- = \{x \in \mathcal{L} : \langle f_1(x), f_2(x) \rangle < 0\}$.

and the sets \mathcal{R}^+ and \mathcal{R}^- similarly:

$$\mathcal{R}^+ = \{x \in \mathbb{R}^2 : \det[f_1(x) \ f_2(x)] > 0\},$$

$$\mathcal{R}^- = \{x \in \mathbb{R}^2 : \det[f_1(x) \ f_2(x)] < 0\}.$$

By assessing whether a point is in \mathcal{R}^+ or \mathcal{R}^- , the field vector giving a chosen edge of the cone can always be identified. The following definition for a new vector field then becomes possible.

Definition 8: The **extremal vector fields** $f_R(x)$ and $f_L(x)$ are defined as

$$f_L(x) = \begin{cases} f_1(x) & x \in \mathcal{R}^+ \\ f_2(x) & x \in \mathcal{R}^- \end{cases}, \quad f_R(x) = \begin{cases} f_2(x) & x \in \mathcal{R}^+ \\ f_1(x) & x \in \mathcal{R}^- \end{cases}.$$

The subscript L and R indicates to which side of the vector the rest of the cone lies.

Solutions of the extremal fields exist everywhere on the plane, and are unique almost everywhere.¹ The trajectories of extremal solutions on the plane are called **extremal arcs**, with trajectories of $f_L(x)$ being called **L-arcs** and trajectories of $f_R(x)$ **R-arcs**.

The boundary of the invariance kernel \mathcal{S}^* is composed of concatenations of extremal arcs that pass through special points. Theory has been advanced to prove this assertion [21], which can be rigorously justified given some generic assumptions on \mathcal{S} and the vector fields [22]. Further, it has been shown that these special points and arcs can be computed via an algorithm having a finite number of steps [21],[22]. In order to apply the algorithm, three additional definitions are necessary.

Definition 9: A connected subset of $\partial\mathcal{S}$ along which both $f_1(x)$ and $f_2(x)$ point inside of \mathcal{S} or are tangent to $\partial\mathcal{S}$ is said to be an **invariant arc of $\partial\mathcal{S}$** . Each endpoint of an invariant arc of $\partial\mathcal{S}$ is called a **t^∂ point**. An invariant arc contains these endpoints and is thus closed.

This definition specifies the character of any endpoint t^∂ of an invariant arc. An endpoint is a point in the curve $\partial\mathcal{S}$ that is the boundary between two connected subsets of the curve. In one subset, both $f_1(x)$ and $f_2(x)$ point inside of \mathcal{S} , while in the other at least one of the fields points out. If $\partial\mathcal{S}$ is differentiable (i.e. is a class \mathcal{C}^1 curve) in a neighborhood of a t^∂ point, then at least one of the vector fields $f_1(x)$, $f_2(x)$ must be there tangent to $\partial\mathcal{S}$.

The orientation of the extremal arcs is already given by the time parametrization of the corresponding extremal solutions, so that the orientation indicates the direction of increasing time. We give $\partial\mathcal{S}$ a positive orientation so that a point moving along $\partial\mathcal{S}$ finds the interior of \mathcal{S} to its left-hand side.

At an equilibrium point \bar{x} of $f_1(x)$ or $f_2(x)$, we define two special types of extremal arcs. Recall that by Definition 8, an extremal arc will coincide with the trajectory on the plane of a solution of either $f_1(x)$ or $f_2(x)$.

Definition 10: Suppose that \bar{x} is an equilibrium of $f_1(x)$ (resp., $f_2(x)$). An extremal arc through \bar{x} is said to be an **equilibrium extremal arc through \bar{x}** if on a neighborhood of \bar{x} it coincides with a trajectory of $f_1(x)$ (resp., a trajectory of $f_2(x)$). If, instead, the extremal arc coincides with a trajectory of $f_2(x)$ (resp., a trajectory of $f_1(x)$) in a neighborhood of \bar{x} , then it is said to be a **non-equilibrium extremal arc through \bar{x}** .

¹Two solutions may converge or diverge from a point $x_0 \in \mathcal{L}^-$, where $f_1(x)$ and $f_2(x)$ are antiparallel. Also the extremal vector fields f_L , f_R are discontinuous on \mathcal{L} . However, the existence and uniqueness of extremal solutions has been discussed in detail in [22] and is supported by the body of work on differential equations with discontinuous right hand side pioneered by Filippov [23].

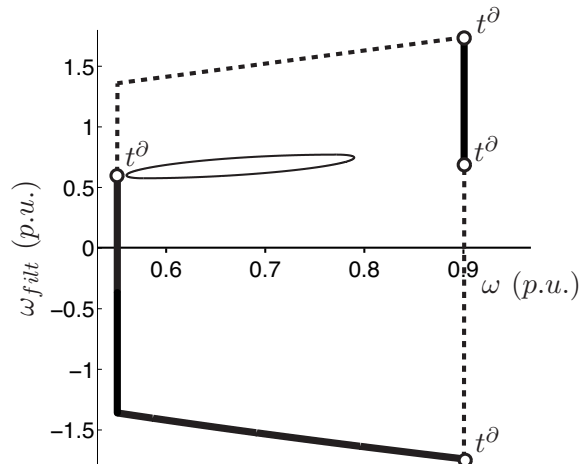


Fig. 11. Identification of special points (open circles) and closed extremal arc (thin solid). Invariant arcs of ∂S (thick solid) are bounded by t^δ points within ∂S (dashed).

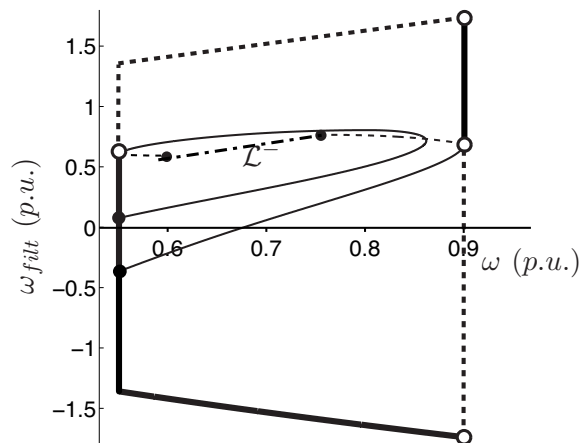


Fig. 12. Integration from special points (open circles) until stopping conditions reached (filled circles).

Definition 11: A point p in \mathcal{L}^- is called a t^- **point** if the trajectories of $f_1(x)$ and $f_2(x)$ through p remain in the closure of \mathcal{R}^+ or the closure of \mathcal{R}^- for some time interval containing $t = 0$ (i.e., $\langle f_1, f_2 \rangle$ has constant sign along the trajectories of $f_1(x)$ and $f_2(x)$ through p for small time).

B. Computing \mathcal{S}^* for Wind Turbine Providing Smoothing

Based on the definitions of the previous section, an algorithm has been devised to compute the invariance kernel in a finite number of steps. The algorithm is stated in the Appendix and has been rigorously justified in an earlier publication [22]. It is assumed that any closed extremal arcs are known. The validity of the algorithm rests on eight generic assumptions on \mathcal{S} and the vector fields, all of which

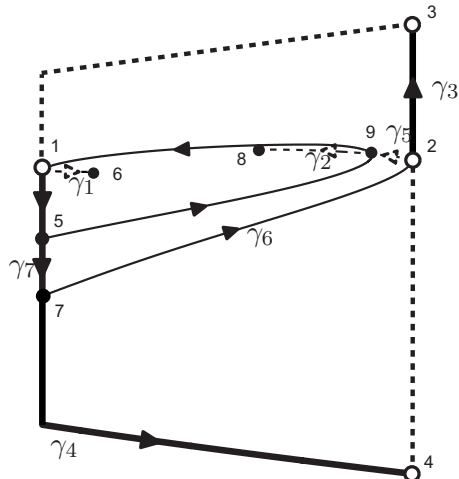


Fig. 13. Point numbering, arc partitioning and pruning (axes omitted for clarity). Arcs $\gamma_1, \dots, \gamma_7$ will be pruned.

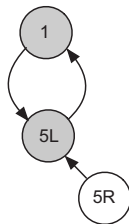


Fig. 14. Vertices and edges of graph G constructed after pruning. One cycle exists (gray vertices).

are met by the simplified wind turbine model.

The algorithm is applied in this section to find the invariance kernel \mathcal{S}^* of the safety set \mathcal{S} as defined in (16), under the dynamics of the wind turbine model (7) with parameters given in [11]. For this example, $\bar{v}_w = 6.4m/s$, $\lambda = 7.43$, $\Delta = 0.700$, and $\tau = 4s$.

1) **Initialization** (Fig. 11):

For the operating point and filter parameter chosen for this example, t^∂ points are the only special points found; the equilibria are foci, and there are no t^- points. There is one closed extremal arc of $f_L(x)$. Fig. 11 shows the objects identified in the initialization step of the algorithm.

2) **Integration** (Fig. 12)

Of the four t^∂ points, only two require integration. Both of them are at the tail of an invariant arc (see Fig. 11), with $f_L(t^\partial)$ tangent to the boundary. This corresponds to the first entry of Table I.

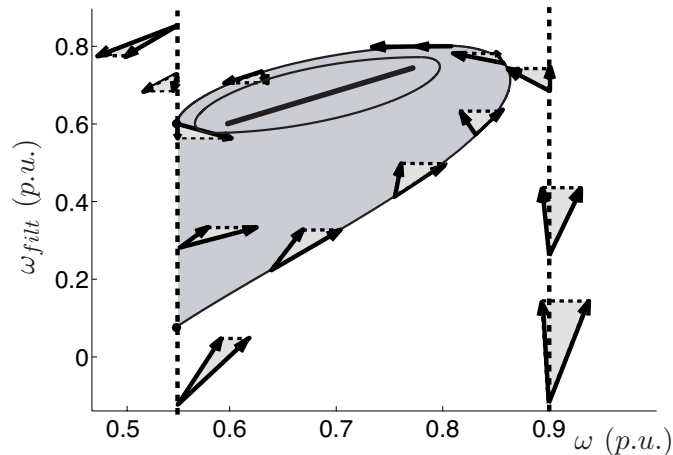


Fig. 15. Invariance kernel S^* (shaded region) identified by the algorithm contains the closed extremal arc, which in turn contains the equilibrium set \mathcal{E} (solid black line). Cone of possible directions is depicted at multiple points (arrows).

Therefore the L-arc through each point is integrated in reverse time (solid arcs) and the R-arc is integrated in forward time. As shown in Fig. 12, the L-arcs (thin solid) hit invariant arcs of ∂S (thick solid), while the R-arcs (thin dashed) hit \mathcal{L}^- .

3) Pruning (Fig. 13)

Fig. 13 shows points and oriented arcs resulting from carrying out the labeling and partitioning of Step 3. There are no arcs sharing the same two endpoints, so there is no action for Step 3.2.

Pruning proceeds in several executions as follows:

EXEC. 1: STEP 3.3: γ_1, γ_2 STEP 3.4: γ_3, γ_4

EXEC. 2: STEP 3.3: γ_5 STEP 3.4: γ_6

EXEC. 3: STEP 3.3: γ_7 STEP 3.4: NO ACTION

No action is required for step 3.6, and in step 3.7 the points 2, 3, 4, 6, 7, 8 and 9 are removed.

4) Graph Construction (Fig. 14)

Fig. 14 shows the results of applying the rules of Step 4. A single vertex has been created for t^∂ point 1 (by 4.1), while two are created for the integration endpoint 5 (by 4.2). The only arcs remaining after pruning are either L-arcs or invariant arcs, so step 4.3 is applied. Graph edges are added from v_1 to v_5^L and from v_5^L to v_1 , forming the only cycle in the graph. Step 4.5 is applied to the significant point 5 so that an edge is added from v_5^R to v_5^L .

5) Cycle Analysis (Fig. 15)

From the graph, there is one cycle that corresponds to a closed curve in the plane composed of an

invariant arc of ∂S and an L-arc, which we will refer to as a concatenation. From the initialization step, there was also a closed extremal arc. Both of these closed curves are plotted in Fig. 15. The union of the regions enclosed by these two closed curves is the invariance kernel, shaded in Fig. 15. As a verification, Fig. 15 also depicts the cone of directions at several points along ∂S and ∂S^* , showing that, indeed, S^* is positively invariant while S is not.

VI. WIND DISTURBANCE MARGIN COMPUTATION: GENERAL CASE

To practically determine \mathcal{M} , one can set the disturbance bound Δ to a small value and then increase it incrementally, finding the planar invariance kernel S^* at each step. As stated in Definition 5, the largest value of Δ for which S^* is both not empty and also contains \mathcal{E} is the wind disturbance margin \mathcal{M} .

A. Computation for Single Value of τ

Fig. 16 demonstrates the incremental process of computing \mathcal{M} for a single value of τ . The invariance kernel S^* is plotted for increasing values of $\Delta \in [0.700, 0.807]$. The closed extremal curve produced in Step 1 of the algorithm expands, while the concatenation produced by Steps 2-4 contracts. The concatenation and the closed extremal curve coincide for the value of $\Delta = 0.807 \text{ m/s}$. Beyond this critical value, S^* is empty. The wind disturbance margin $M(\bar{v}_w, \Delta)$ is therefore equal 0.807 m/s .

The important arc of the concatenation is the trajectory passing through points 1, 9 and 5 in Fig. 13. That trajectory intersects itself when $\Delta = \mathcal{M}$. This observation could lead to a more direct method of computing \mathcal{M} based on analyzing the sensitivity of the trajectory in question. However, different critical trajectories will determine \mathcal{M} for other parameter values of \bar{v}_w , λ_* , and τ . The incremental process is a flexible approach that can be generally applied.

B. Results for Range of τ

The disturbance margin as determined through the incremental process over a range of τ is plotted in Fig. 17(a) for $\lambda_* = \lambda_{opt}$ and in Fig. 17(b) for $\lambda_* = 8.62$ (a de-loading of 20%). The margins for the extreme cases $\tau = 0$ and $\tau = \infty$ have been computed from (18) and (24) and plotted as horizontal lines for comparison.

For small values of τ , the margin approaches the value calculated for the limiting case of $\tau = 0$ for both choices of de-loading. For large values of τ , the margin approaches zero for the selection $\lambda_* = \lambda_{opt}$, and approaches the quantity (21) for the de-loaded selection. The analysis of planar invariance kernels is required to describe anything other than the asymptotic behaviour of the disturbance margin. Without

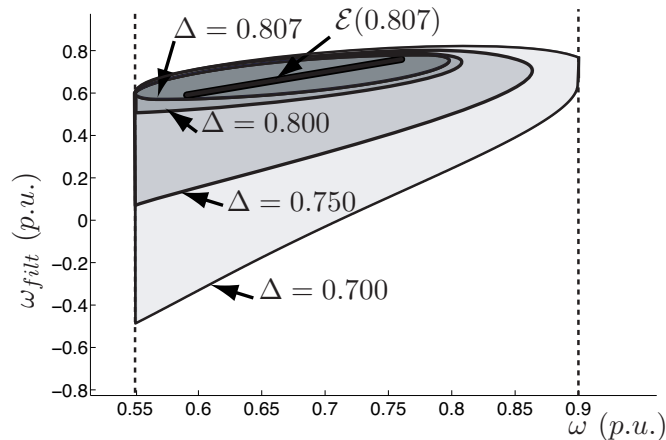


Fig. 16. Computation of \mathcal{M} for a single value of τ by incrementing Δ and finding invariance kernels (shaded). $\bar{v}_w = 6.4m/s, \lambda_* = 7.43, \tau = 4s$.

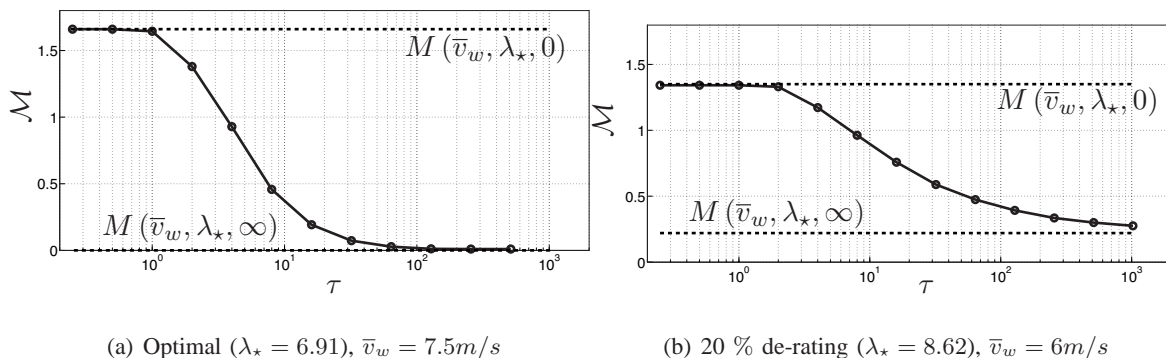


Fig. 17. $M(\bar{v}_w, \lambda_*, \tau)$ over a range of $\tau \in [0, \infty]$ (solid with dots), compared with special cases obtained from analysis of torque-speed intersections (dashed) for degenerate cases $\tau = 0$ (using (18)) and $\tau = \infty$ (using (24)).

such analysis, one could not be sure that smoothing operation would be stable, particularly in the case of $\lambda = \lambda_*$. The ability to compute the margin makes it possible to find the largest allowable τ for a given range of expected wind disturbance, or vice-versa.

VII. CONCLUSIONS AND FUTURE WORK

This paper has introduced an efficient method of rigorously studying the behaviour of wind turbines that implement power smoothing by exploiting the kinetic energy of the rotor. It was argued that traditional approaches to analyzing machine dynamics are not adequate for studying the problem. It was shown that by performing a number of integrations of the dynamical equations of a simplified model from certain special points, it is possible to determine whether a given control law will produce acceptably bounded

behaviour in response to a class of bounded wind variations. By applying this new method to determine the largest safe bound on such wind variations, the concept of a disturbance margin for the controlled wind turbine has been quantified.

The disturbance margin enables a systematic design of τ to obtain maximal smoothing within available freedom. In this paper it has been used to prove that smoothing operation can be stable without de-loading. These two results could not be obtained using the traditional technique of speed torque intersection analysis. Using the new techniques and disturbance margin concept introduced in this paper, a model of the wind turbine's maximal smoothing capability over its operating range could be created. Such models could be combined with information about expected turbulence intensity to evaluate the availability of the smoothing capability over a chosen time period. A practical evaluation would likely not be based on the absolute range of the signal, but on a chosen fraction of its probability mass, so as to indicate highly probable rather than guaranteed smoothing capability.

The benefit of the disturbance margin introduced in this paper is a quantification of the robustness of a given control law. The method presented here for finding the invariance kernel allows computation of the disturbance margin for any system that can be formulated as a planar nonlinear affine control system. This can now be used to compare different control laws or different wind turbine technologies on a common basis of equal robustness, and in future to inform on-line adjustments of control parameters in response to wind conditions to safely maximize exploitation of wind turbine kinetic energy.

APPENDIX

A. Sufficient Conditions on $h(x, u)$

The theory presented and applied in this paper is proven in [22] using the properties of the linearization at equilibria of $f_1(x)$ and $f_2(x)$. For the linearization to exist, the vector fields (31) and (32) must be differentiable in x at equilibria. Ensuring this requires analysis of the function $h(x, u)$, whose maximum and minimum values h_{min} and h_{max} are obtained a given point x with the inputs

$$\xi_{min}(x) = \arg \min_{u \in [u_{min}, u_{max}]} h(x, u) \quad (34)$$

$$\xi_{max}(x) = \arg \max_{u \in [u_{min}, u_{max}]} h(x, u). \quad (35)$$

By the chain rule, we also require differentiability at equilibria from the minimizing and maximizing functions $\xi_{min}(x)$ and $\xi_{max}(x)$. For (7) these requirements are sufficiently satisfied by the strong property

that $h(x, u)$ is monotonically dependent on u in the domain of interest. For, where ever

$$\left. \frac{\partial}{\partial u} h(\mathbf{x}, u) \right|_{x,u} \geq 0 \quad (36)$$

then functions $\xi_{min}(x)$ and $\xi_{max}(x)$ are constant and equal to the minimum and maximum values of the input u :

$$\xi_{min}(\mathbf{x}) = u_{min} \quad (37)$$

$$\xi_{max}(\mathbf{x}) = u_{max} \quad (38)$$

Considering the function $h(x, u)$ for (7), as given by (30):

$$\begin{aligned} \left. \frac{\partial}{\partial u} C_p \left(\frac{k_4 x_1}{u} \right) u^3 \right|_{x_1^*, u^*} = & \quad (39) \\ \left[-\frac{dC_p}{d\lambda} \frac{k_4 x_1^*}{u^{*2}} u^{*3} + 3C_p \left(\frac{k_4 x_1^*}{u^*} \right) u^{*2} \right] & \end{aligned}$$

the substitution

$$\lambda^* = \frac{k_4 x_1^*}{u^*} \quad (40)$$

allows a simplification showing the derivative (39) is equal zero when

$$\lambda^* = \frac{3C_p(\lambda^*)}{\left. \frac{dC_p}{d\lambda} \right|_{\lambda^*}} \quad (41)$$

which for $C_p(\lambda)$ can happen at two values of λ . For the aerodynamic model [11] studied here, (36) holds for all $\lambda^* \in [4, 16.9]$. The domain of wind speeds $v_w \in [4, 11]$ and rotor speeds $\omega \in [0.92, 1.5]$ studied here imply, by the tip-speed ratio (1), a maximum possible range of $\lambda^* \in [3.5, 15.8]$, and thus the condition (41) is never violated.

B. Algorithm to Find Planar Invariance Kernel S^*

1. Initialization

Determine:

- 1.1. t^∂ points in \mathcal{S} ,
- 1.2. t^- points in \mathcal{S} ,
- 1.3. nodes and saddles of f_1 or f_2 in \mathcal{S} ,
- 1.4. closed extremal arcs in \mathcal{S} .

2. Integration

Initial condition		extremal arc	integration direction
t^∂ point, tail of inv. arc	f_L is tangent	L	rev.
		R	fwd.
	f_R is tangent	do nothing	
t^∂ point, head of inv. arc	f_L is tangent	do nothing	
	f_R is tangent	L	fwd.
		R	rev.
t^- point		L	fwd.
		L	rev.
		R	fwd.
		R	rev.
node stable or (unstable)		non-eq	fwd.
			rev.
		eq., fast manifold	rev. (fwd.) rev. (fwd.)
saddle		non-eq	fwd.
			rev.
		eq., stable manifold	rev.
			rev.
		eq.,unstable manifold	fwd.
		fwd.	

TABLE I

RULES OF INTEGRATION THROUGH SPECIAL POINTS.

Using the integration rules in Table I, generate extremal arcs from all points computed in Part 1.

The stopping criteria for the integration are:

- 2.1. The solution hits \mathcal{L}^- at a point which is not a t^- point.
- 2.2. The solution hits ∂S at a point which does not lie on an invariant arc of ∂S .
- 2.3. The solution hits an invariant arc of ∂S coming from $\text{int } S$.
- 2.4. The solution is detected to reach (in finite or infinite time) an equilibrium of f_1 or f_2 or to spiral (in positive or negative time) around a limit set.

3. Pruning

Label all points identified in Part 1 (steps 1.1-1.4) as *special points*. Label as *significant* all special

points, all the integration endpoints, and all points of intersection between extremal arcs generated in Part 2 or between extremal and invariant arcs of ∂S . Thus, special points are significant, but not vice versa.

- 3.1. Partition each extremal arc resulting from an integration performed in Part 2 and invariant arcs of ∂S into sub-arcs whose heads and tails are the significant points. The sub-arcs inherit the orientation of the parent arc. In the rest of the algorithm below, these sub-arcs will be simply referred to as extremal arcs.
- 3.2. Prune one L-arc γ and one R-arc η if γ and η have the same endpoints, and if neither endpoint is special.
- 3.3. Prune any L-arc (resp. R-arc) with head at a point p which is not special if there is no L-arc (resp., R-arc) with tail at p .
- 3.4. Prune any extremal arc whose head or tail is at a point where no other arc is connected.
- 3.5. Repeat steps 3.3-3.4 until there is not more arc to prune.
- 3.6. Prune extremal arcs that spiral around limit sets in positive or negative time.
- 3.7. Eliminate from the list of significant points all points with no arcs attached, and points connecting only two arcs of the same type (L or R).

4. Graph construction

Construct a graph $G = (V, E)$, with V the set of vertices of G and E the set of edges of G as follows.

Vertices of G . Let \mathcal{P} denote the set of significant points in \mathcal{S} that remain after the pruning in Part 3.

- 4.1. For every point $p \in \mathcal{P}$ which is special, create a vertex v_p .
- 4.2. For every $p \in \mathcal{P}$ which is not special, create two vertices, denoted v_p^L and v_p^R .

Edges of G . Create directed edges between vertices associated with extremal arcs and invariant arcs of ∂S as follows:

- 4.3. If p is the tail of an L-arc or an invariant arc of ∂K with head at q , create a directed edge from v_p , or v_p^L , to v_q , or v_q^L .
- 4.4. If p is the tail of an R-arc with head at q , create a directed edge from v_q , or v_q^R , to v_p , or v_p^R .
- 4.5. For every (v_p^L, v_p^R) pair, create a directed edge from v_p^R to v_p^L .

5. Cycle Analysis

- 5.1. Find all simple cycles (i.e., closed paths that do not visit any vertex more than once) in the

graph G .

- 5.2. Discard any cycles containing two vertices v_p^R, v_p^L that are not consecutive (when travelling in the direction of the edges of the graph).
- 5.3. For each remaining cycle in G , check whether the region in the plane delimited by the path associated to the cycle is positively or negatively invariant. If it is negatively invariant, discard the cycle.
- 5.4. \mathcal{S}^* is the union of all regions enclosed by closed paths associated to graph cycles and by closed extremal trajectories in \mathcal{S} .

Remark 1: The test in step 5.3 can be done simply by picking any non-special point p in the closed path and discarding the cycle if $f_1(p)$ points outside the region delimited by the path.

REFERENCES

- [1] T. Burton, D. Sharpe, N. Jenkins, and E. Bossanyi. *Wind Energy Handbook*. Wiley, 2001.
- [2] L.Ran, J.R. Bumby, and P.J. Tavner. Use of turbine inertia for power smoothing of wind turbines with a DFIG. In *11th International Conference on Harmonics and Quality of Power*, pages 106–111, September 12–15 2004.
- [3] B. Rawn, P.W. Lehn, and M. Maggiore. A control methodology to mitigate the grid impact of wind turbines. *IEEE Transactions on Energy Conversion*, 22(2):431–438, June 2007.
- [4] C.L. Luo, H. Banakar, B. Shen, and B.T. Ooi. Strategies to smooth wind power fluctuations of wind turbine generator. *IEEE Transactions on Energy Conversion*, 22(2):243–349, June 2007.
- [5] T.Luu, A.Abedini, and A. Nasiri. Power smoothing of doubly fed induction generator wind turbines. *Industrial Electronics, 2008. IECON 2008. 34th Annual Conference of IEEE*, pages 2365 – 2370, 2008.
- [6] C. Jauch and T. Cronin. Simulation model of a wind turbine pitch controller for grid frequency stabilization. *Wind Engineering*, 29(4):377–387, 2005.
- [7] F.M. Hughes, O. Anaya-Lara, N. Jenkins, and G. Strbac. A power system stabilizer for DFIG-based wind generation. *IEEE Transactions on Power Systems*, 21(2):763–772, 2006.
- [8] J. Morren, J. Pierik, and S. W. H de Haan. Inertial response of variable speed wind turbines. *Electric Power System Research*, 76:980–987, 2006.
- [9] J. Ekanayake and N. Jenkins. Comparison of the response of doubly fed and fixed-speed induction generator wind turbines to changes in network frequency. *IEEE Transactions on Energy Conversion*, 19(4):800–802, 2004.
- [10] N. Wang, K. Johnson, and A. Wright. FX-RLS-based feedforward control for LIDAR-enabled wind turbine load mitigation. *Control Systems Technology, IEEE Transactions on*, (99):1–11, 2011.
- [11] J. G. Sloopweg, H. Polinder, W. L. Kling, and J.A Ferreira. Representing wind turbine electrical generating systems in fundamental frequency simulation. *IEEE Transactions on Energy Conversion*, 18(4):516–524, December 2003.
- [12] E. Muljadi and C.P Butterfield. Pitch-controlled variable-speed wind turbine generation. *IEEE Transactions on Industry Applications*, 37(1):240–246, Jan/Feb 2001.
- [13] E.A Bossanyi. Wind turbine control for load reduction. *Wind Energy*, 6(3):229–244, 2003.

- [14] K.A. Mary, A. Patra, N.K. De, and S. Sengupta. Design and implementation of the control system for an inverter-fed synchronous motor drive. *Control Systems Technology, IEEE Transactions on*, 10(6):853–859, 2002.
- [15] W.E. Leithead, S. de la Salle, and D. Reardon. Roles and objectives of control for wind turbines. *IEE Proceedings-C*, 138(2):135–148, 1991.
- [16] P. Fleming E. A. Bossanyi, A. Wright. Controller field tests on the NREL CART3 Turbine. *Project Upwind Integrated Wind Turbine Design*, 2009.
- [17] AD Wright, LJ Fingersh, and KA Stol. Designing and testing controls to mitigate tower dynamic loads in the Controls Advanced Research Turbine. In *45th AIAA Aerospace Sciences Meeting and Exhibit, Wind Energy Symposium, Reno, Nevada (USA)*, 2007.
- [18] B. Connor W.E. Leithead. Control of variable speed wind turbines: dynamic models. *International Journal of Control*, 73(13):1173–1188, 2000.
- [19] A.M. Howlader, N. Urasaki, T. Senjyu, A. Uehara, A. Yona, and AY Saber. Output power smoothing of wind turbine generation system for the 2-mw permanent magnet synchronous generators. In *Electrical Machines and Systems (ICEMS), 2010 International Conference on*, pages 452–457. IEEE, 2010.
- [20] N. Miller, W. Price, and J. Sanchez-Gasca. Dynamic modelling of ge 1.5 and 3.6 mw wind-turbine generators. *Version 3.0 Technical Report*, 2003.
- [21] B. Rawn. *Ensuring Safe Exploitation of Wind Turbine Kinetic Energy: An Invariance Kernel Formulation*. Ph.D. Thesis, Department of Electrical and Computer Engineering, University of Toronto, 2009.
- [22] M. Maggiore, B. Rawn, and P. Lehn. Invariance kernels of single-input planar nonlinear systems. *SIAM Journal on Control and Optimization*, Accepted for publication, December 2011.
- [23] A.F. Filippov and F.M. Arscott. *Differential Equations with Discontinuous Righthand Sides*. Springer, 1988.



Barry G. Rawn (M '10) received the PhD degree in electrical engineering in 2010 from the University of Toronto, where he also received the B.A.Sc. and M.A.Sc. degrees in Engineering Science and Electrical Engineering. His research interests include nonlinear dynamics and sustainable energy infrastructure. He is currently a postdoctoral researcher in the Electrical Power Systems group at the Delft University of Technology, The Netherlands.



Peter Lehn (SM,'05) received the B.Sc. and M.Sc. degrees in electrical engineering from the University of Manitoba, Winnipeg, MB, Canada, in 1990 and 1992, respectively, and the Ph.D. degree from the University of Toronto, Toronto, ON, Canada, in 1999. From 1992 to 1994, he was with the Network Planning Group, Siemens AG, Erlangen, Germany. He is currently a Professor at the University of Toronto. His research interests include modeling and control of converters and integration of renewable energy sources into the power grid.



Manfredi Maggiore (M '99) was born in Genoa, Italy. He received the "Laurea" degree in Electronic Engineering in 1996 from the University of Genoa and the PhD degree in Electrical Engineering from the Ohio State University, USA, in 2000. Since 2000 he has been with the Edward S. Rogers Sr. Department of Electrical and Computer Engineering, University of Toronto, Canada, where he is currently Associate Professor. He has also been a visiting Professor at the University of Bologna (2007-2008). His research focuses on mathematical nonlinear control, and relies on methods from dynamical systems theory and

differential geometry.